Title

Flexible Zn-MOF with Rare Underlying scu Topology for Effective Separation of C6 Alkane Isomers

Journal

ACS Applied Materials & Interfaces, 13(44)

ISSN

1944-8244

Authors

Velasco, Ever

Xian, Shikai

Wang, Hao

et al.

Publication Date

2021-11-10

DOI

10.1021/acsami.1c08678

A flexible Zn-MOF with rare underlying *scu* topology for effective separation of C6 alkane isomers

Ever Velasco,[a] Shikai Xian,[a,b] Hao Wang,[b] Simon J. Teat,[c] David H. Olson,[a] Kui Tan,[d] Saif Ullah,[e] Thomas Osborn Popp,[a] Ashley Bernstein,[a] Kolade A. Oyekan,[d] Andrew J. Nieuwkoop,[a] Timo Thonhauser [e] and Jing Li [a,*]

[a] Department of Chemistry and Chemical Biology, Rutgers University, 123 Bevier Road, Piscataway, New Jersey 08854, USA

[b] Hoffmann Institute of Advanced Materials, Shenzhen Polytechnic, 7098 Liuxian Boulevard., Shenzhen, Guangdong 518055, China

[c] Advanced Light Source Lawrence Berkeley National Laboratory, 1 cyclotron Road, Berkeley, California 94720, USA

[d] Department of Materials Science & Engineering, University of Texas at Dallas, 800 Campbell Road, Richardson, Texas 75080, USA

[e] Department of Physics and Center for Functional Materials, Wake Forest University, 1834 Wake Forest Road, Winston-Salem, North Carolina 27109, USA

KEYWORDS Metal-organic framework (MOF), kinetic separation, molecular sieving, hydrocarbon, flexible structure, alkane isomers
Supporting Information Placeholder

ABSTRACT: Adsorptive separation by porous solids provides an energy efficient alternative for the purification of important chemical species compared to energy intensive distillations. Particularly, the separation of linear hexane isomers from its branched counterparts is crucial to produce premium grade gasoline with high research octane number (RON). Herein, we report the synthesis of a new, flexible zinc-based metal-organic framework, $[Zn_5(\mu 3\text{-}OH)_2(adtb)_2(H_2O)_5 \cdot 5\ DMA]$ (Zn-adtb), constructed from a butterfly shaped carboxylate linker with underlying 4,8 - connected ***scu*** topology capable of separating the C6 isomers *n*HEX, 3MP and 23DMB. The sorbate-sorbent interactions and separation mechanism were investigated and analyzed through in-situ FTIR, solid state NMR measurements and computational modeling. These studies reveal that Zn-adtb discriminates the *n*HEX/3MP isomer pair through a kinetic separation mechanism and the *n*HEX/23DMB isomer pair through a molecular sieving mechanism. Column breakthrough measurements further demonstrate the efficient separation of linear *n*HEX from the mono- and di- branched isomers.

INTRODUCTION

Chemical separation of small hydrocarbons is crucial to society as it provides critical chemical precursors to produce widely demanded commodities such as polymers, plastics, and gasoline. Within the petrochemical industry, C6 isomers are of particular interest because they play a key role in controlling the overall quality of gasoline. The catalytic isomerization reactions used on distilled naphtha streams obtained from the oil refinement processes of crude petroleum produce a mixture of C5 and C6 isomers. These isomers are used as ingredients in gasoline, however, to produce premium grade quality gasoline, it is important that the additives and contents of the gasoline have high research octane number (RON).[1] The three C6 isomers, linear n-hexane (*n*HEX), single branched 3-methylpentane (3MP) and di-branched 2,3 dimethylbutane (23DMB) have RON values of 30, 74.5 and 101.7, respectively.[2] For aliphatic hydrocarbons, the RON values typically increase with the degree of branching for the isomers. Therefore, to produce premium grade quality gasoline it is imperative to separate the linear isomer from its branched relatives. However, the separation of C6 isomer mixtures is challenging by virtue of their similar chemical and physical properties.[3-5] Currently, the separation of *n*HEX from its branched isomers is achieved through energy intensive heat-driven distillation. In this purification process, crude naphtha mixtures are heated to temperatures ranging from 35-200 °C and distillates are collected in large distillation towers. However, the similarity in physical boiling point of these isomers sometimes requires multiple distillations to provide isomers of high enough purity. As an alternative to heat-driven distillation, adsorptive separation with porous solids provides a more energetically efficient route for the

purification of C6 isomers. However, the separation of these aliphatic isomers with sorbent materials remains challenging because their chemical properties and kinetic diameters are quite similar.[1] These similarities complicate sorbent based chemical separation techniques that rely either on a thermodynamic mechanism that is governed by the adsorbate-adsorbent interactions, a kinetic based separation mechanism that is governed by adsorption kinetics, or a molecular sieving mechanism that is based on the size exclusion. Currently, the only commercialized solid adsorbent material in use for the separation of C6 isomers is zeolite 5A and serves only as a supplement to the resulting distillates of naphtha from heat-driven distillation partly because of its drawbacks such as low *n*HEX uptake amounts and poor functionalizability.[6-7] These limitations of zeolite 5A prompt researchers to continue the search for solid sorbent materials with higher uptake capacities and better selectively.

Metal-Organic Frameworks (MOFs) have been extensively studied for gas storage,[8-11] separation,[12-18] capture of hazardous chemical species,[19-21] catalysis,[22-24] conductivity,[25-28] luminescence sensing,[29-33] and lighting[34-39] applications because of their permanent porosity and ease of tunability with regards to their pore shape, size, and chemistry.[40-41] The facile functionalization of MOFs makes them versatile and attractive materials for numerous applications. The versality of MOFs stems from the individual components used to synthesize this class of materials. MOFs are porous, crystalline materials constructed from inorganic primary building units (PBUs) or secondary building units (SBUs) strut together by organic linkers through coordinative bonds to produce 3D, extended networks. With practically unlimited combinations of metal ions and organic linkers it is easy to understand their versatile nature. The separation of hydrocarbons ranging from C2 to C8 through solid sorbent materials has seen extensively explored in the past decade. Researchers have sought to develop materials that no longer rely on thermodynamic and kinetic separations and instead make use of the ideal, extreme case scenario of kinetic separation, namely full molecular size exclusion, where only one isomer can enter the pore of a sorbent material while other isomers are too large to enter the pore aperture, thus providing the highest separation selectivity. Materials for the separation of isomers through a molecular sieving effect for C6 isomers are quite rare. Currently, there are only four MOFs reported for the molecular sieving of C6 isomers.[14, 42-44]

Herein, we present a new, flexible three-dimensional (3D) MOF $[Zn_5(\mu 3\text{-}OH)_2(adtb)_2(H_2O)_5 \cdot 5DMA]$ (**1**), denoted as Zn-adtb (H_4adtb=4,4',4'',4'''-(anthracene-9,10-diylidenebis(methanediylylidene))tetrabenzoic acid) constructed from a butterfly shaped and highly distorted organic linker. Zn-adtb crystallizes in a reported, yet rare ***scu*** topology for Zn-based MOFs. It is capable of selectively discriminating and separating C6 alkane isomers. At 300 K, it selectively adsorbs ~120 mg/mmol of *n*HEX but only 20 mg/mmol of the single branched isomer 3MP and 5 mg/mol of the di-branched isomer 23 DMB. The mechanism of separation was revealed to be kinetic based separation for *n*HEX/3MP and molecular sieving for *n*HEX/23DMB through computational modeling and in-situ FTIR and solid state NMR measurements. Furthermore, the separation efficiency of the Zn-adtb was confirmed with breakthrough experiments using an equimolar ternary mixture of C6 isomers.

EXPERIMENTAL SECTION

Materials

All general reagents and solvents were obtained from commercially available sources and used without further purification unless specifically mentioned. The organic linker and precursors were synthesized following previously published literature with minor modifications,[45-47] detailed synthesis conditions may be found in the electronic supplementary information (ESI).

Synthesis of Zn-adtb (1)

Zinc(II) nitrate hexahydrate ($Zn(NO_3)_2 \cdot 6\ H_2O$, 32 mg, 0.11 mmol) was ultrasonically dissolved in 2 mL of N',N' Dimethylacetamide (DMA) until a clear solution was formed. After which, 1 mL of distilled water was added to the reaction solution. Lastly, H_4adtb (30 mg, 0.044 mmol) was then added to the solution and sonicated for 5 minutes before being placed in a preheated oven at 373 K. After 48 hours, the clear, rod shaped single crystals were collected after being filtrated and washed thoroughly with DMA (Figure S1). Approximately 20 mg (40.13% yield based on Zn) of Zn-adtb crystal sample was obtained.

Sample Activation

Approximately 100 mg of **1** was washed 5 times with 20 mL portions of DMA, Dichloromethane (DCM) and then bulk n-hexanes, each. Samples were not allowed to dry during the DCM solvent exchange steps. Lastly, the sample was activated under dynamic vacuum for 8 hours at 373 K.

Characterization

Powder X-ray Diffraction (PXRD) measurements were obtained from 3-40° (2θ) with a scan speed of 1° min^{-1} using a copper k_α radiation source (λ = 1.5406 Å) using a Rigaku Ultima-IV X-ray diffractometer at room temperature. The thermogravimetric analysis (TGA) was collected by loading ~10 mg of a sample on a platinum pan with a heating rate of 10 °C min^{-1} from room temperature to 700 °C on a TA instruments Q5000IR analyzer under a constant flow of nitrogen and sample purge rate of 10 ml/min and 12 ml/min, respectively. Carbon dioxide adsorption isotherms were collected at 195 K on a Micromeritics 3Flex adsorption analyzer. Prior to isotherm measurements, ~100 mg of Zn-adtb was solvent exchanged (see sample activation section) and heated to 100 °C under a dynamic vacuum for 12 hours. Proton NMR of the organic linkers and their

precursors were obtained from a 300 MHz Oxford NMR.

Adsorption Experiments

Single component isotherms and adsorption rates for *n*HEX, 3MP and 23DMB were collected in a homemade gravimetric adsorption analyzer modified from a TGA Q50 (TA instruments). The bubbler containing the hydrocarbon ran ultra-high purity N_2 as the carrier gas. The partial pressure of the specific C6 hydrocarbon isomer was adjusted by controlling the ratio of pure N_2 gas and the N_2 gas that was saturated with the C6 isomer for the experiment. Approximately 20 mg of Zn-adtb was activated under a constant N_2 flow for 4 hours at 373 K. Adsorbed amounts of individual hydrocarbons were monitored by weight changes in the sample and continuously monitored throughout the experiments. Kinetic adsorption rates were collected at their specified temperatures for approximately 1 to 2 hours.

Solid State NMR Experiments

Solid-state NMR studies of the as-made MOF with and without added DMA were acquired on a 9.4 T Bruker Avance III spectrometer equipped with a Bruker 3.2 mm HXY probe tuned to HCN, with a frequency of 400.203 MHz for 1H and 100.640 MHz for 13C. All spectra were acquired at 25°C and 20 kHz MAS. For all experiments the 1H 90° pulse length was 2.55 µs and the 13C 90° pulse length was 4.00 µs. CP experiments were acquired with 4096 scans, with a 2 s recycle delay and either 0.1 or 2 ms contact time. 1H spectra were acquired with 4 scans each with a recycle delay of 5 s. 13C HETCOR spectra were acquired with 64 points in the indirect dimension with a dwell time of 8 µs, with 512 scans per increment, a recycle delay of 4 s, and a contact time of 2 ms. Solid-state NMR studies of the activated and C6 isomer-loaded samples were acquired on a 14.1 T Bruker Avance III spectrometer equipped with an HXYD 1.6 mm Phoenix probe tuned to HC double resonance mode, with a frequency of 599.684 MHz for 1H and 150.797 MHz for 13C. Spectra were acquired at 20°C and at either 15 or 20 kHz MAS. A 90° pulse length of 1.459 µs was used for 1H and 2.040 µs for 13C. 1H 1D spectra were acquired with 4 scans and a recycle delay of 2.5 s. CP experiments were acquired with 4096 scans, a recycle delay of 2 s, and 2 ms contact time. 13C HETCOR spectra were acquired with 64 pts in the indirect dimension with a dwell time of 5.333 µs, with 128, 256, or 400 scans per increment, a recycle delay of 2 s, and a contact time of 2

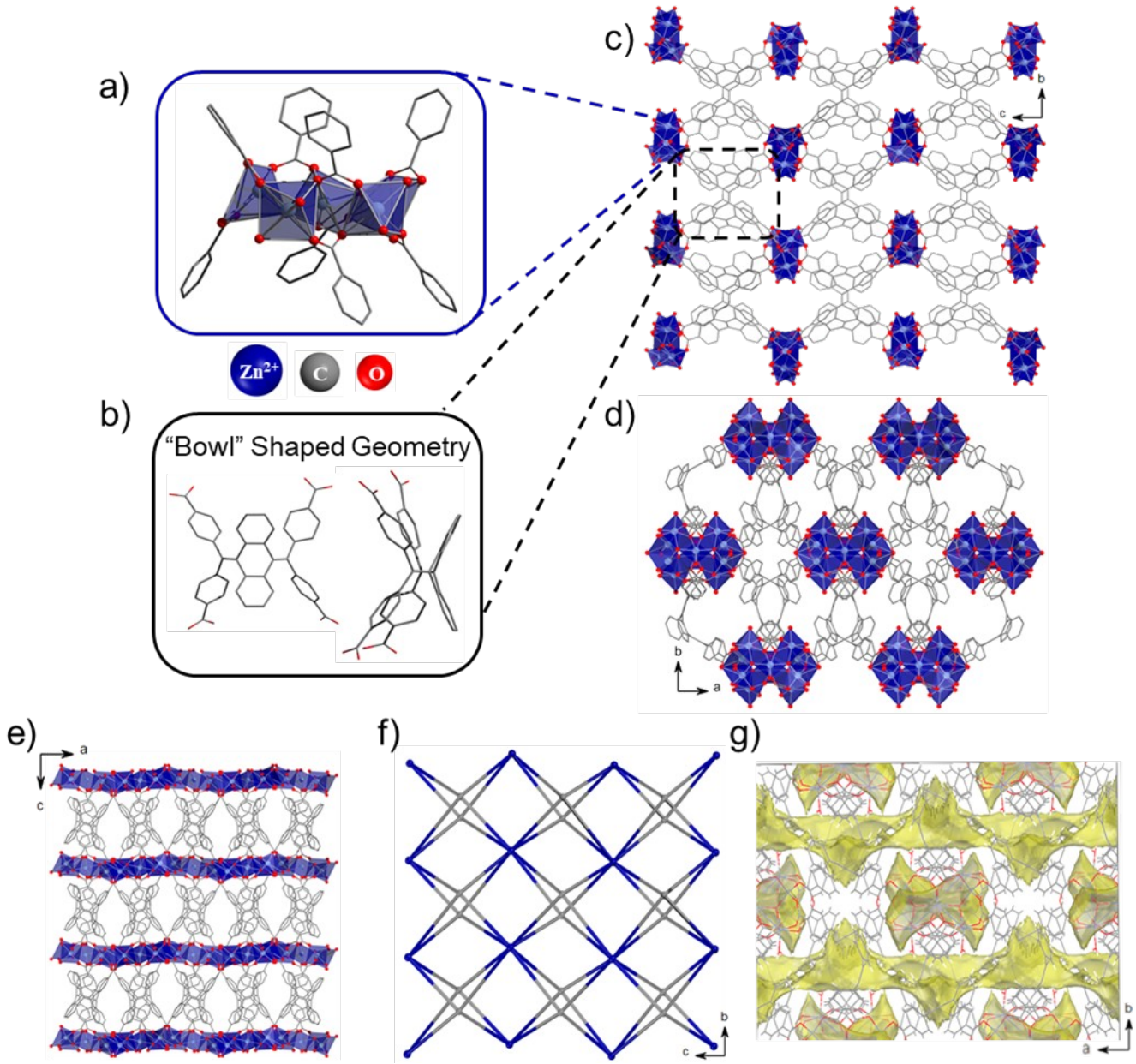

Figure 1. Crystal structure of compound 1 (a) The entanuclear eight connected secondary building unit (SBU) of **1**. (b) The organic linker H_4adtb in a front and side view. (c-e) The perspective view of structure **1** along the crystallographic a-, b- and c-axis, respectively. (f) The topological breakdown of **1** depicting the overall 4,8 connected **scu** topology. (g) Schematic representation of the interconnected pore system within **1** running in the direction of the crystallographic a-axis.

ms. For all samples, chemical shifts were referenced to adamantane (13C downfield peak 38.48 ppm, 1H resonance 1.74 ppm). The magic angle was set with KBr by maximizing the magnitude of the 1st order spinning sideband of 79Br. 1D spectra were processed using TopSpin version 3.6.1 and 2D spectra were processed withNMRPipe and CCPN Analysis. Samples run on the 9.4 T Bruker spectrometer were packed into 3.2 mm Bruker reduced volume zirconia rotors (Cortecnet, Paris-Saclay, France). Samples run on the 14.1 T Bruker spectrometer were packed into 1.6 mm zirconia rotors (Phoenix NMR, Loveland, CO). All samples were packed in air at room temperature. In order to add DMA, n-hexane, or 3-methylpentane to the rotors, the cap was removed and 4 µL or 10 µL of the desired solvent was added via pipette to the 1.6 mm and 3.2 mm rotors respectively, before being quickly recapped. The rotors were allowed to equilibrate for several hours or overnight before being placed into the spectrometer for data acquisition.

Breakthrough Experiments

Column breakthrough measurement was performed with a lab-scale fix-bed reactor at 30 °C. 0.65 g of sample **1** was packed into a quartz column (4.0 mm I.D. ×300 mm) with silane treated glass wool filling the void space. A nitrogen flow (5 mL min^{-1}) was used to purge the adsorbent. The powder sample

was activated at 100 °C for 6 hours and the flow of nitrogen was then turned off while another dry nitrogen flow at a rate of 1 mL/min was bubbled through a mixture of hexane isomers according to the following volumes (the volumes were determined through trial and error and calculated by GC: the experiment was run without any sample and the vapor phase ratios were optimized to an equimolar mixture): 6.12 mL of nHEX, 4.36 mL of 3MP, and 2.89 mL of 23DMB for nHEX/3MP/23DMB ternary mixture (partial pressure of each component is 50 torr). The effluent from the column was monitored using an online GC equipped with HP-PONA column and FID.

Table 1. Single Crystal Data for Zn-adtb

In-Situ FTIR Measurements

In situ IR measurements were performed on a Nicolet 6700 FTIR spectrometer using a liquid N2-cooled mercury cadmium telluride (MCT-A) detector. A vacuum cell is placed in the sample compartment of the infrared spectrometer with the sample at the focal point of the beam. The sample (~5 mg) were gently pressed onto KBr pellet and placed into a cell that is connected to a vacuum line for evacuation. The sample were activated by evacuation overnight at 30 ºC for C6 alkane isomer vapor exposure measurement. After each exposure, the sample was evacuated under vacuum overnight for regeneration.

Computational Modeling

First-principles density functional theory calculations with the van der Waals density functional (vdW-DF1)[48-51] were performed to assess the interactions between C6 alkanes and the Zn-MOF using the VASP code.[52-53] The plane-wave cutoff was set to 500 eV and projected augmented wave (PAW) pseudopotentials were used. Due to the large unit cell size with 684 atoms, only the Γ-point was sampled. We used a fully crystalline model of the MOF with periodic boundary conditions. The convergence criteria were set to 10-6 eV and 10-2 eV/Å for energies and forces, respectively. Binding energies were calculated as the difference between the energies of the fragments (C6 isomers + empty MOF) and the loaded MOF.

RESULTS AND DISCUSSION

Structural Analysis

Single crystal analysis of the rod-shaped single crystals reveal that Zn-adtb crystallizes in the orthorhombic crystal system, space group *Pbcn*. The framework contains a discrete inorganic secondary building unit (SBU) composed of a pentanuclear Zn cluster with the molecular formula $[Zn_5(\mu^3\text{-}OH)_2(COO)_8(H_2O)_4]$ (Figure 1, Table 1). Within the SBU, there are a total of three crystallographic unique Zn atoms, Zn_1, Zn_2 and Zn_3. Out of the five Zn atoms in the SBU, there are two 5-coordinated Zn_1 atoms with 4 bonds to organic linkers and one bond to a μ^3-O that bridges to the nearest Zn atom. Additionally, there are two Zn_2 atoms that possess a 6-coordinated environment with 3 bonds to organic linkers, one bond to a μ^3-O and the remaining two bonds to two terminal water molecules. Lastly, there is a single Zn_3 atom with a 6-coordinated environment where 4 bonds pertain to the organic linker and two bonds to μ^3-O. Every pentanuclear cluster is coordinated to eight individual organic linkers. The organic linker H_4adtb takes on a bowl-shaped, highly distorted geometry (Figure 1b) and each of its four carboxylate groups coordinate to a different Zn cluster, resulting in a 3D extended network (Figure 1c, d, e). The organic linkers in the structure are overall 4-connected and topological analysis with TOPOS reveals that Zn-adtb packs in the (4,8) - connected ***scu*** topology with the Schlaefli symbol $\{4^{16} \cdot 6^{12}\}\{4^4 \cdot 6^2\}_2$ (Figure 1f). However, late-transition metal and post-transition metal (such as Cu^{2+} and Zn^{2+}) based MOFs featuring ***scu*** topology have been rarely reported (Table S1). Furthermore, each inorganic SBU contains a total of 4 terminally coordinated water molecules that point directly into the resulting 1D channel along the a-axis of the structure (Figure 1g). Despite the differences in the metal of the inorganic SBU, the pentanuclear Zn cluster in Zn-adtb and hexanuclear Zr cluster in Zr-abtc have the same overall connectivity resulting in the same topology. Previous work has shown the effectiveness of Zr-abtc, a 4,8 connected MOF with ***scu*** topology, for the separation of 3MP from 23 DMB; however, the 1D channel is large enough to accommodate *n*HEX, 3MP and 23DMB. Thus, separation of the two isomers occurs via a thermodynamic based mechanism.[42] While the overall topology of the two structures is the same, and both contain 1D open channels, the pore structures in Zn-adtb and Zr-abtc are quite different. In Zr-abtc, the structure is formed by a relatively planar tetratropic linker H_4abtc (3,3',5,5'-azobenzene-tetracarboxylate) that bridges nearby Zr-nodes. The planarity of the organic linker limits the linkers protrusion into the pore aperture of the structure. However, in Zn-adtb, the highly bent and distorted butterfly linker H_4adtb takes on a bowl-shaped geometry that allows the backbone of the organic linker to protrude into the pore aperture of the structure. The effect of this protrusion reflects as a reduction in both the pore aperture and BET surface area of the material. This overall reduction in pore size led us to believe that the material may be feasible as an adsorbent for the separation of C6 isomers or alkane isomers with shorter chain length. Indeed, Zn-adtb demonstrates clear separation of the linear *n*HEX isomer from the mono- and di-branched isomers via kinetic or size exclusion mechanisms with high uptake capacity for the linear nHEX isomer.

Crystal Data	
Compound	Zn-adtb (**1**)
Formula	$Zn_5C_{108}N_5O_{29}H_{107}$
M	2265.83
Crystal system	orthorhombic
Space group	Pbcn
a (Å)	16.1783 (8)
b (Å)	24.8432 (12)
c (Å)	26.2068 (13)
α	90
β	90
γ	90
V (Å^3)	10533.1 (9)
Z	4
Temperature	100
λ (radiation	0.7749
D (g/cm^3)	1.429
Reflections	9484
R1[I > 2σ(1)]	0.0381
wR2 [I > 2σ(1)]	0.1073
Goodness-of-fit	1.051
CCDC no.	2067421

Stability, Porosity and Structural Transformation

The bulk phase purity of Zn-adtb was confirmed by powder X-ray diffraction (PXRD) analysis where the diffraction pattern of the as-made Zn-adtb matches well with the simulated pattern (Figure 2a). The permanent porosity of Zn-adtb was estimated using CO_2 absorption isotherm data since this material displays essentially no N_2 uptake at 77K. Activation was accomplished by thoroughly washing the as-made sample with DMA and solvent exchanging with dichloromethane (DCM) then by bulk n-hexanes according to a previously published technique,[54] followed by activation at 373 K

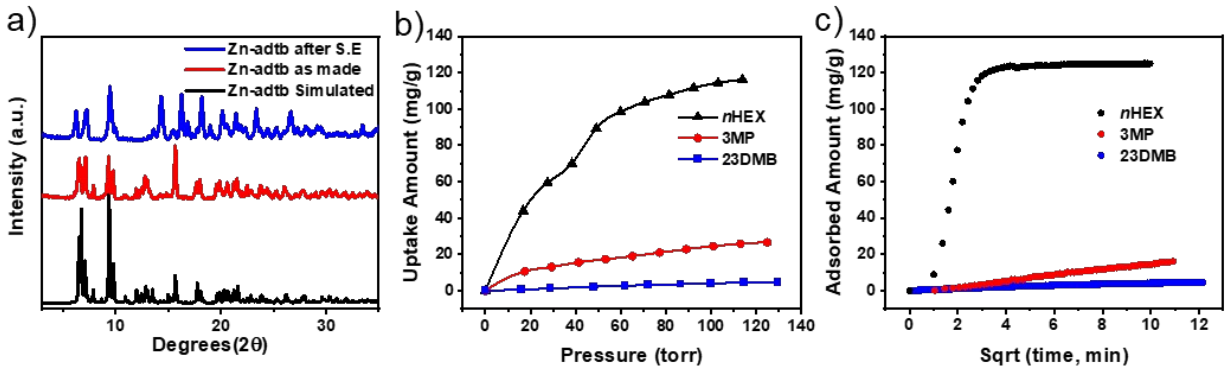

Figure 2. (a) The PXRD patterns of simulated, as-made and solvent exchanged Zn-adtb depicting the structural changes that occur through each step. (b) The *n*HEX, 3MP and 23DMB adsorption isotherms at 30 ˚C. (c) The adsorption rates of *n*HEX, 3MP and 23 DMB at 30 ˚C.

under vacuum for 8 hours. CO_2 isotherms show a typical type I isotherm with no hysteresis and an uptake amount of approximately 120 cm^3/g of CO_2 at 195 K (Figure S2). From the CO_2 adsorption isotherms, we can obtain the Brunauer-Emmett-Teller (BET) surface area of ~273 m^2/g, which deviates from the theoretical BET surface area of 388 m^2/g from the crystal structure. The experimental and theoretical BET surface areas do not match well because upon solvent exchange and activation Zn-adtb undergoes a structural transformation as seen from the PXRD patterns (Figure 2a and Figure S3). The discrepancy between the theoretical calculations and experimental values occurs because the calculations for the porosity of a material assume that the material is rigid and does not undergo structural changes during activation. We then explored the thermal stability of Zn-adtb through thermogravimetric Analysis (TGA). The results show that both the as-made Zn-adtb and the

sample after solvent exchange remained stable until ~450 ℃ (Figure S4). We then evaluated the chemical stability of Zn-adtb by exposing the as-made sample to aqueous solutions of various pH values (1-12) for 72 hours and PXRD patterns were then collected. As seen from Figure S5, the PXRD patterns of **1** confirmed that the compound retains high crystallinity under these conditions, demonstrating its high stability in chemical environments.

Single Component Adsorption of Hexane Isomers

From the single component isotherms, we determined that the uptake amounts of the linear *n*HEX isomer in Zn-adtb are 120 mg/g, 80 mg/g and 66 mg/g at 30 °C, 60 °C and 90 °C, respectively (Figure S6). The adsorption isotherms at 60 °C and 90 °C display a typical fully reversible type I isotherm. However, the adsorption isotherm at 30 °C shows a S-shaped section where the uptake capacity increases rapidly up to ~30 torr, then the adsorption rate slows down from ~20 torr to 30 torr, before increasing again at 40 torr. Such adsorption behavior is typical of flexible MOFs and has been observed in the adsorption of hexane isomers in other flexible structures such as Ca(H_2tcpb).[43] From the adsorption isotherms and rates at 30 °C, we can see that the uptake amounts for the linear *n*HEX, the mono-branched 3MP and di-branched 23DMB are ~120 mg/g, 20 mg/g and 5 mg/g (Figure 2b). The linear *n*HEX adsorption rates hit equilibrium rapidly (~9 mins) while the mono-branched 3MP shows very slow adsorption rate and di-branched 23DMB reveals essentially no adsorption (Figure 2c). These data suggest that the separation of 3MP and 23DMB may be effectively achieved by a kinetic and molecular sieving process, respectively. To determine whether the adsorption of the C6 isomers occurs through a kinetic or size exclusion-based mechanism at different temperatures, we measured adsorption rates for *n*HEX/3MP/23DMB at 30, 60 and 90 °C. From Figure S7, we can see that the adsorption of *n*HEX reaches equilibrium rapidly at ~9 mins while the uptake capacity decreases as the temperature increases and does not display diffusion-based restrictions. On the other hand, the uptake amount of 3MP increases from 10 mg/g to 15 mg/g to 25 mg/g as the temperature increases from 30 °C to 60 °C to 90 °C, respectively without reaching equilibrium (Figure S8). This behavior is typical of a kinetic based separation mechanism as the diffusivity of 3MP increases as a function of temperature. For 23DMB, the rate curves show low uptake capacity that does not increase as a function of temperature, suggesting a molecular sieving separation for the much larger dibranched isomer (Figure S9). The small uptake amounts of 23DMB may be attributed to either defect or surface-based interactions. To assess the recyclability of this material we performed multiple cycles of adsorption and desorption of *n*HEX using the same sample. As seen in Figures S10 and S11, there is no depreciable decrease in uptake amount of *n*HEX even after 6 cycles.

Breakthrough Experiments

In the forgoing section we have investigated the adsorption of C6 alkane isomers by Zn-adtb by single component adsorption isotherm and adsorption kinetics experiments. The results reveal that Zn-adtb shows distinct adsorption behavior to hexane isomers with different branching: it adsorbs substantial amount of nHEX but negligible uptake of its mono- and di-branched isomers under identical conditions, as a result of its restricted pore dimensions. To further evaluate the separation capability of Zn-adtb under real-world conditions, we carried column breakthrough measurements with a 1:1:1 ternary mixture of nHEX, 3MP, and 23DMB at 30 ℃. It can be seen from the breakthrough curve that the MOF material exhibits a clear separation of *n*HEX from its branched isomers 3MP and 23DMB. 23DMB eluted immediately out from the column at the beginning of the measurements, followed by 3MP, consistent with their negligible uptake amounts in the single component adsorption isotherms. In contrast, *n*HEX was retained in the column for ~30 minutes before it broke out. These results suggest that Zn-adtb represents another and rare MOF adsorbents that is capable of full separation of linear C6 isomer from the branched ones.[14, 42-43]

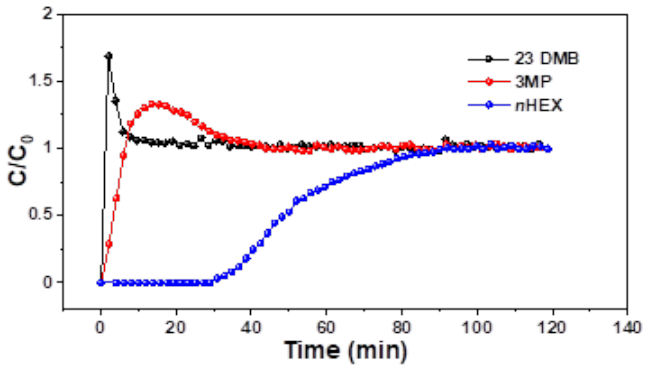

Figure 3. The breakthrough curves using an equimolar ternary mixture of *n*HEX, 3MP and 23DMB at 30° C.

Solid State NMR

Discussions

In-situ FTIR Analysis

To examine the interaction between these C6 isomers and Zn-adtb, we have employed *in situ* infrared spectroscopy to measure the loading of C_6 isomers and the response of Zn-adtb's vibrational modes. As shown in the difference spectra of Figure 4b, the adsorption of C6 isomers is typified by their characteristic hydrocarbon stretching bands ν(-CH_2, CH_3) at 3000-2800 cm^{-1}. Meanwhile, we see clear perturbation of the bands associated with middle phenyl ring including CC stretching, CH in-plane and out-of-plane deformation as well as stretching and

bending vibrations of water, pointing to their interaction with loaded C_6 isomers and the terminal water. The most pronounced perturbation occurs upon loading n-HEX, which is consistent with our following calculation that shows that nHEX binds most strongly inside Zn-adtb.

Computational Modeling

Various C6 alkanes were loaded in the pore site and their binding energies were calculated. We find that the binding strength is inversely related to the kinetic diameter of the C6 alkanes. The strongest binding is found for the linear isomer *n*HEX, closely followed by the monobranched 3MP. Additionally, moderate binding energy is calculated for the dibranched alkanes 22DMB and 23DMB. The large size of the unit cell prohibits the use of transition-state calculations. To mimic an approximate transition state and find the corresponding energy barrier, we calculated the energy for a configuration where the H_2O is at the aperture of the MOF pore (closing off a significant portion of the chamber) and compare it with a configuration where the H_2O is in the pore. Using this approach, for *n*HEX we find an estimated diffusion barrier of 0.15 eV, easily overcome at room temperature and suggesting that *n*HEX can easily diffuse through the MOF network. However, 3MP faces substantial opposition at the aperture with an estimated diffusion barrier of 0.45 eV, resulting in a significant reduction in uptake compared to *n*HEX. Finally, for the di-branched isomers 22DMB and 23DMB— due to their large kinetic diameters—we find that they cannot pass through the aperture.

CONCLUSIONS

In conclusion, we have successfully synthesized a new Zn-based MOF with a bowl-shaped butterfly linker. The microporous structure packs in a (4,8) – connected extended network with ***scu*** topology, a rare topology for Zn-based MOFs. Single component isotherms and adsorption rates of C6 alkane isomers reveal that at room temperature Zn-adtb demonstrates efficient separation of the linear *n*HEX from the mono- and di- branched 3MP and 23DMB isomers, respectively. The uptake amounts for *n*HEX, 3MP and 23 DMB from the adsorption rates at room temperature are 120 mg/g, 20 mg/g and 5 mg/g, respectively. Our columns breakthrough experiments demonstrate the efficient separation of the linear from branched isomers with breakthrough times of 2 minutes, 8 minutes and 31 minutes for *n*HEX, 3MP and 23DMB, respectively. Our computational modeling and in-situ FTIR measurements reveal that

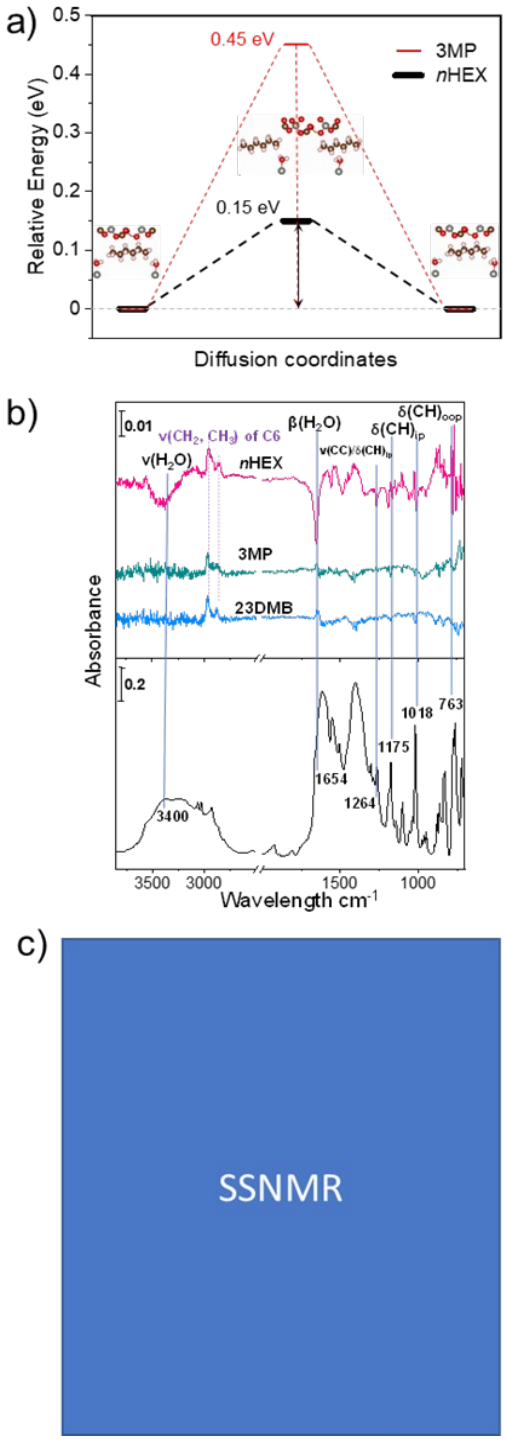

Figure 4. (a) Diffusion barrier for *n*HEX and 3MP. The maximum of the barrier occurs at the pore aperture of the MOF. (b) Difference spectra of Zn-adtb sample exposed to *n*HEX (pink), 3MP (green) and 23DMB (blue) vapor at ~8 Torr, respectively, referenced to the spectrum of pristine sample under vacuum (black). The spectra of gas phase of C6 isomers were substracted. Notation and acronyms: ν, stretching; δ, deformation; β, bending; ip, in plane; oop, out of plane. The mode assignment is established by DFT calculation (see Figure S11). (c)

the separation mechanism for *n*HEX/3MP occurs through a kinetic separation mechanism where the large diffusion barrier of 3MP through the pore aperture results in an appreciable decrease in diffusivity of 3MP in the material. However, the separation mechanism for *n*HEX/23DMB follows molecular sieving whereby the kinetic diameter of 23 DMB is too large to diffuse through the pore aperture of the MOF.

ASSOCIATED CONTENT

Supporting Information

The single crystal data, organic linker synthesis, thermogravimetric analysis and additional plots for this manuscript is available free of charge via the Internet at http://pubs.acs.org.

AUTHOR INFORMATION

Corresponding Author

Jing Li - Department of Chemistry and Chemical Biology, Rutgers University, 123 Bevier Road, Piscataway, New Jersey, 08854, USA

Author Contributions

The manuscript was written through contributions of all authors. All authors have given approval to the final version of the manuscript.

Notes

The authors declare no competing financial interests.

ACKNOWLEDGMENT

This work was supported by the U. S. Department of Energy, Office of Science, Office of Basic Energy Sciences under Award No. DE-SC0019902. This research used resources of the Advanced Light Source, which is a DOE Office of Science User Facility under contract no. DE-AC02-05CH11231.

REFERENCES

1. Myers, R. A., *Handbook of Petroleum Refining Processes*. McGraw-Hill, New York: 2004.
2. Schenk, M.; Vidal, S. L.; Vlugt, T. J. H.; Smit, B.; Krishna, R., Separation of Alkane Isomers by Exploiting Entropy Effects during Adsorption on Silicalite-1: A Configurational-Bias Monte Carlo Simulation Study. *Langmuir* **2001,** *17* (5), 1558-1570.
3. Herm, Z. R.; Bloch, E. D.; Long, J. R., Hydrocarbon Separations in Metal–Organic Frameworks. *Chemistry of Materials* **2014,** *26* (1), 323-338.
4. Zhou, F.; Liang, Y.; Liu, W., Ionic liquid lubricants: designed chemistry for engineering applications. *Chemical Society Reviews* **2009,** *38* (9), 2590-2599.
5. Bárcia, P. S.; Silva, J. A. C.; Rodrigues, A. E., Adsorption equilibrium and kinetics of branched hexane isomers in pellets of BETA zeolite. *Microporous and Mesoporous Materials* **2005,** *79* (1), 145-163.
6. Jasra, R. V.; Bhat, S. G. T., Adsorptive Bulk Separations by Zeolite Molecular Sieves. *Separation Science and Technology* **1988,** *23* (10-11), 945-989.
7. Peralta, D.; Chaplais, G.; Simon-Masseron, A.; Barthelet, K.; Pirngruber, G. D., Separation of C6 Paraffins Using Zeolitic Imidazolate Frameworks: Comparison with Zeolite 5A. *Industrial & Engineering Chemistry Research* **2012,** *51* (12), 4692-4702.
8. Liu, J.; Thallapally, P. K.; McGrail, B. P.; Brown, D. R.; Liu, J., Progress in adsorption-based CO2 capture by metal–organic frameworks. *Chemical Society Reviews* **2012,** *41* (6), 2308-2322.
9. Sanz-Pérez, E. S.; Murdock, C. R.; Didas, S. A.; Jones, C. W., Direct Capture of CO2 from Ambient Air. *Chemical Reviews* **2016,** *116* (19), 11840-11876.
10. Sumida, K.; Rogow, D. L.; Mason, J. A.; McDonald, T. M.; Bloch, E. D.; Herm, Z. R.; Bae, T.-H.; Long, J. R., Carbon Dioxide Capture in Metal–Organic Frameworks. *Chemical Reviews* **2012,** *112* (2), 724-781.
11. Ding, M.; Flaig, R. W.; Jiang, H.-L.; Yaghi, O. M., Carbon capture and conversion using metal–organic frameworks and MOF-based materials. *Chemical Society Reviews* **2019,** *48* (10), 2783-2828.
12. Yang, S.; Ramirez-Cuesta, A. J.; Newby, R.; Garcia-Sakai, V.; Manuel, P.; Callear, S. K.; Campbell, S. I.; Tang, C. C.; Schröder, M., Supramolecular binding and separation of hydrocarbons within a functionalized porous metal–organic framework. *Nature Chemistry* **2015,** *7* (2), 121-129.
13. Li, L.; Guo, L.; Zhang, Z.; Yang, Q.; Yang, Y.; Bao, Z.; Ren, Q.; Li, J., A Robust Squarate-Based Metal–Organic Framework Demonstrates Record-High Affinity and Selectivity for Xenon over Krypton. *Journal of the American Chemical Society* **2019,** *141* (23), 9358-9364.
14. Chen, Q.; Xian, S.; Dong, X.; Liu, Y.; Wang, H.; Olson, D. H.; Williams, L. J.; Han, Y.; Bu, X.-H.; Li, J., High-Efficiency Separation of n-Hexane by a Dynamic Metal-Organic Framework with Reduced Energy Consumption. *Angewandte Chemie International Edition* **2021,** *n/a* (n/a).
15. Wang, H.; Li, J., Microporous Metal–Organic Frameworks for Adsorptive Separation of C5–C6 Alkane Isomers. *Accounts of Chemical Research* **2019,** *52* (7), 1968-1978.
16. Wang, H.; Liu, Y.; Li, J., Designer Metal–Organic Frameworks for Size-Exclusion-Based Hydrocarbon Separations: Progress and Challenges. *Advanced Materials* **2020,** *32* (44), 2002603.
17. Wang, H.; Warren, M.; Jagiello, J.; Jensen, S.; Ghose, S. K.; Tan, K.; Yu, L.; Emge, T. J.; Thonhauser, T.; Li, J., Crystallizing Atomic Xenon in a Flexible MOF to Probe and Understand Its Temperature-Dependent Breathing Behavior and Unusual Gas Adsorption Phenomenon. *Journal of the American Chemical Society* **2020,** *142* (47), 20088-20097.
18. Wang, H.; Dong, X.; Colombo, V.; Wang, Q.; Liu, Y.; Liu, W.; Wang, X.-L.; Huang, X.-Y.; Proserpio, D. M.; Sironi, A.; Han, Y.; Li, J., Tailor-Made Microporous Metal–Organic Frameworks for the Full Separation of Propane from Propylene Through Selective Size Exclusion. *Advanced Materials* **2018,** *30* (49), 1805088.
19. Li, B.; Dong, X.; Wang, H.; Ma, D.; Tan, K.; Jensen, S.; Deibert, B. J.; Butler, J.; Cure, J.; Shi, Z.; Thonhauser, T.; Chabal, Y. J.; Han, Y.; Li, J., Capture of organic iodides from nuclear waste by metal-organic framework-based molecular traps. *Nature Communications* **2017,** *8* (1), 485.
20. Rudd, N. D.; Wang, H.; Fuentes-Fernandez, E. M. A.; Teat, S. J.; Chen, F.; Hall, G.; Chabal, Y. J.; Li, J., Highly Efficient Luminescent Metal–Organic Framework for the Simultaneous Detection and Removal of Heavy Metals from Water. *ACS Applied Materials & Interfaces* **2016,** *8* (44), 30294-30303.
21. Jensen, S.; Tan, K.; Feng, L.; Li, J.; Zhou, H.-C.; Thonhauser, T., Porous Ti-MOF-74 Framework as a Strong-Binding Nitric Oxide Scavenger. *Journal of the American Chemical Society* **2020,** *142* (39), 16562-16568.
22. An, B.; Li, Z.; Song, Y.; Zhang, J.; Zeng, L.; Wang, C.; Lin, W., Cooperative copper centres in a metal–organic framework for selective conversion of CO2 to ethanol. *Nature Catalysis* **2019,** *2* (8), 709-717.

23. Zhu, C.; Yue, H.; Jia, J.; Rueping, M., Nickel-Catalyzed C-Heteroatom Cross-Coupling Reactions under Mild Conditions via Facilitated Reductive Elimination. *Angewandte Chemie International Edition* **2020,** *n/a* (n/a).
24. Wen, Y.; Feng, M.; Zhang, P.; Zhou, H.-C.; Sharma, V. K.; Ma, X., Metal Organic Frameworks (MOFs) as Photocatalysts for the Degradation of Agricultural Pollutants in Water. *ACS ES&T Engineering* **2021**.
25. Ren, X.; Liao, G.; Li, Z.; Qiao, H.; Zhang, Y.; Yu, X.; Wang, B.; Tan, H.; Shi, L.; Qi, X.; Zhang, H., Two-dimensional MOF and COF nanosheets for next-generation optoelectronic applications. *Coordination Chemistry Reviews* **2021,** *435*, 213781.
26. Han, B.-X.; Jiang, Y.-F.; Sun, X.-R.; Li, Z.-F.; Li, G., Proton conductive N-heterocyclic metal–organic frameworks. *Coordination Chemistry Reviews* **2021,** *432*, 213754.
27. Liu, H.; Wang, Y.; Qin, Z.; Liu, D.; Xu, H.; Dong, H.; Hu, W., Electrically Conductive Coordination Polymers for Electronic and Optoelectronic Device Applications. *The Journal of Physical Chemistry Letters* **2021,** *12* (6), 1612-1630.
28. Meng, H.; Han, Y.; Zhou, C.; Jiang, Q.; Shi, X.; Zhan, C.; Zhang, R., Conductive Metal–Organic Frameworks: Design, Synthesis, and Applications. *Small Methods* **2020,** *4* (10), 2000396.
29. Hu, Z.; Deibert, B. J.; Li, J., Luminescent metal–organic frameworks for chemical sensing and explosive detection. *Chemical Society Reviews* **2014,** *43* (16), 5815-5840.
30. Hu, Z.; Lustig, W. P.; Zhang, J.; Zheng, C.; Wang, H.; Teat, S. J.; Gong, Q.; Rudd, N. D.; Li, J., Effective Detection of Mycotoxins by a Highly Luminescent Metal–Organic Framework. *Journal of the American Chemical Society* **2015,** *137* (51), 16209-16215.
31. Lustig, W. P.; Mukherjee, S.; Rudd, N. D.; Desai, A. V.; Li, J.; Ghosh, S. K., Metal–organic frameworks: functional luminescent and photonic materials for sensing applications. *Chemical Society Reviews* **2017,** *46* (11), 3242-3285.
32. Velasco, E.; Osumi, Y.; Teat, S. J.; Jensen, S.; Tan, K.; Thonhauser, T.; Li, J., Fluorescent Detection of Carbon Disulfide by a Highly Emissive and Robust Isoreticular Series of Zr-Based Luminescent Metal Organic Frameworks (LMOFs). *Chemistry* **2021,** *3* (1).
33. Wang, H.; Lustig, W. P.; Li, J., Sensing and capture of toxic and hazardous gases and vapors by metal–organic frameworks. *Chemical Society Reviews* **2018,** *47* (13), 4729-4756.
34. Gong, Q.; Hu, Z.; Deibert, B. J.; Emge, T. J.; Teat, S. J.; Banerjee, D.; Mussman, B.; Rudd, N. D.; Li, J., Solution Processable MOF Yellow Phosphor with Exceptionally High Quantum Efficiency. *Journal of the American Chemical Society* **2014,** *136* (48), 16724-16727.
35. Liu, X.-Y.; Lustig, W. P.; Li, J., Functionalizing Luminescent Metal–Organic Frameworks for Enhanced Photoluminescence. *ACS Energy Letters* **2020,** *5* (8), 2671-2680.
36. Lustig, W. P.; Shen, Z.; Teat, S. J.; Javed, N.; Velasco, E.; O'Carroll, D. M.; Li, J., Rational design of a high-efficiency, multivariate metal–organic framework phosphor for white LED bulbs. *Chemical Science* **2020,** *11* (7), 1814-1824.
37. Liu, X.-Y.; Xing, K.; Li, Y.; Tsung, C.-K.; Li, J., Three Models To Encapsulate Multicomponent Dyes into Nanocrystal Pores: A New Strategy for Generating High-Quality White Light. *Journal of the American Chemical Society* **2019,** *141* (37), 14807-14813.
38. Lustig, W. P.; Li, J., Luminescent metal–organic frameworks and coordination polymers as alternative phosphors for energy efficient lighting devices. *Coordination Chemistry Reviews* **2018,** *373*, 116-147.
39. Hu, Z.; Huang, G.; Lustig, W. P.; Wang, F.; Wang, H.; Teat, S. J.; Banerjee, D.; Zhang, D.; Li, J., Achieving exceptionally high luminescence quantum efficiency by immobilizing an AIE molecular chromophore into a metal–organic framework. *Chemical Communications* **2015,** *51* (15), 3045-3048.
40. Li, B.; Zhang, Y.; Ma, D.; Shi, Z.; Ma, S., Mercury nano-trap for effective and efficient removal of mercury(II) from aqueous solution. *Nature Communications* **2014,** *5* (1), 5537.
41. Zhang, J.-P.; Zhang, Y.-B.; Lin, J.-B.; Chen, X.-M., Metal Azolate Frameworks: From Crystal Engineering to Functional Materials. *Chemical Reviews* **2012,** *112* (2), 1001-1033.
42. Wang, H.; Dong, X.; Lin, J.; Teat, S. J.; Jensen, S.; Cure, J.; Alexandrov, E. V.; Xia, Q.; Tan, K.; Wang, Q.; Olson, D. H.; Proserpio, D. M.; Chabal, Y. J.; Thonhauser, T.; Sun, J.; Han, Y.; Li, J., Topologically guided tuning of Zr-MOF pore structures for highly selective separation of C6 alkane isomers. *Nature Communications* **2018,** *9* (1), 1745.
43. Wang, H.; Dong, X.; Velasco, E.; Olson, D. H.; Han, Y.; Li, J., One-of-a-kind: a microporous metal–organic framework capable of adsorptive separation of linear, mono- and di-branched alkane isomers via temperature- and adsorbate-dependent molecular sieving. *Energy & Environmental Science* **2018,** *11* (5), 1226-1231.
44. Yu, L.; Dong, X.; Gong, Q.; Acharya, S. R.; Lin, Y.; Wang, H.; Han, Y.; Thonhauser, T.; Li, J., Splitting Mono- and Dibranched Alkane Isomers by a Robust Aluminum-Based Metal–Organic Framework Material with Optimal Pore Dimensions. *Journal of the American Chemical Society* **2020,** *142* (15), 6925-6929.
45. Jia, S.; Xiao, X.; Li, Q.; Li, Y.; Duan, Z.; Li, Y.; Li, X.; Lin, Z.; Zhao, Y.; Huang, W., Tuning the Connectivity, Rigidity, and Functionality of Two-Dimensional Zr-Based Metal–Organic Frameworks. *Inorganic Chemistry* **2019,** *58* (19), 12748-12755.
46. Dorca, Y.; Naranjo, C.; Delgado-Martínez, P.; Gómez, R.; Sánchez, L., Planarization of tetracarboxamides: tuning the self-assembly of polycyclic aromatic hydrocarbons. *Chemical Communications* **2019,** *55* (43), 6070-6073.
47. Donovan, P. M.; Scott, L. T., Elaboration of Diaryl Ketones into Naphthalenes Fused on Two or Four Sides: A Naphthoannulation Procedure. *Journal of the American Chemical Society* **2004,** *126* (10), 3108-3112.
48. Berland, K.; Cooper Vr Fau - Lee, K.; Lee K Fau - Schröder, E.; Schröder E Fau - Thonhauser, T.; Thonhauser T Fau - Hyldgaard, P.; Hyldgaard P Fau - Lundqvist, B. I.; Lundqvist, B. I., van der Waals forces in density functional theory: a review of the vdW-DF method. (1361-6633 (Electronic)).
49. Langreth, D. C.; Lundqvist, B. I.; Chakarova-Käck, S. D.; Cooper, V. R.; Dion, M.; Hyldgaard, P.; Kelkkanen, A.; Kleis, J.; Kong, L.; Li, S.; Moses, P. G.; Murray, E.; Puzder, A.; Rydberg, H.; Schröder, E.; Thonhauser, T., A density functional for sparse matter. *Journal of Physics: Condensed Matter* **2009,** *21* (8), 084203.
50. Thonhauser, T.; Cooper, V. R.; Li, S.; Puzder, A.; Hyldgaard, P.; Langreth, D. C., Van der Waals density functional: Self-consistent potential and the nature of the van der Waals bond. *Physical Review B* **2007,** *76* (12), 125112.
51. Thonhauser, T.; Zuluaga, S.; Arter, C. A.; Berland, K.; Schröder, E.; Hyldgaard, P., Spin Signature of Nonlocal Correlation Binding in Metal-Organic Frameworks. *Physical Review Letters* **2015,** *115* (13), 136402.
52. Kresse, G.; Furthmüller, J., Efficient iterative schemes for ab initio total-energy calculations using a plane-wave basis set. *Physical Review B* **1996,** *54* (16), 11169-11186.

53. Kresse, G.; Joubert, D., From ultrasoft pseudopotentials to the projector augmented-wave method. *Physical Review B* **1999,** *59* (3), 1758-1775.
54. Ma, J.; Kalenak, A. P.; Wong-Foy, A. G.; Matzger, A. J., Rapid Guest Exchange and Ultra-Low Surface Tension Solvents Optimize Metal–Organic Framework Activation. *Angewandte Chemie International Edition* **2017,** *56* (46), 14618-14621.